Estimation of spudcan penetration in variable sand deposits with the Arbitrary Lagrangian Eulerian Finite Element Method

Tolooiyan, Ali; Gavin, Kenneth; Dyson, Ashley P.

DOI
10.1016/j.oceaneng.2023.114955

Publication date
2023

Document Version
Final published version

Published in
Ocean Engineering

Citation (APA)
Tolooiyan, A., Gavin, K., & Dyson, A. P. (2023). Estimation of spudcan penetration in variable sand deposits with the Arbitrary Lagrangian Eulerian Finite Element Method. *Ocean Engineering*, *281*, Article 114955. https://doi.org/10.1016/j.oceaneng.2023.114955

Important note
To cite this publication, please use the final published version (if applicable).
Please check the document version above.

Ocean Engineering 281 (2023) 114955

Contents lists available at ScienceDirect

Ocean Engineering

journal homepage: www.elsevier.com/locate/oceaneng

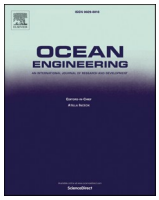

Estimation of spudcan penetration in variable sand deposits with the Arbitrary Lagrangian Eulerian Finite Element Method

Ali Tolooiyan [a,*], Kenneth Gavin [b], Ashley P. Dyson [a]

[a] Computational Engineering for Sustainability Lab (CES-Lab), School of Engineering, University of Tasmania, Hobart, 7005, Australia
[b] Faculty of Civil Engineering and Geosciences, TU Delft, 2628 CN, Delft, the Netherlands

ARTICLE INFO

Handling Editor: Prof. A.I. Incecik

Keywords:
Spudcan
Penetration
FEM
Sand
Jack-up
Arbitrary Lagrangian-Eulerian

ABSTRACT

Offshore jack-up rigs are most commonly founded on large-diameter conical "spudcan" foundations, which are frequently designed using traditional analytical methods for shallow footings. This paper presents the design of a spudcan installed off the coast of Tunisia. The maximum penetration depth of the footing under the available preload is predicted by a combination of analytical techniques, 2-dimensional axisymmetric modelling and 3-dimensional Finite Element Methods (FEM) using large strain arbitrary Lagrangian-Eulerian (ALE) techniques. Spudcan penetration based on FEM simulation of CPT soil profiles forms the basis of a comparison with results from the Society of Naval Architects and Marine Engineers (SNAME) guidelines. Particular attention is given to model calibration using the limited site investigation data available. Results are presented for the effect of penetrating footings on the behaviour of neighbouring footings, showing good agreement with conventional prediction methods.

1. Introduction

Jack-up platforms are used extensively in the offshore oil and gas sectors, with recent implementation in the installation of wind farms in the North and Irish Sea. These vessels typically contain three to four legs, each founded on a large diameter conical footing called a spudcan (Deng et al., 2021). Jack-up legs are lowered until contact is made with the seabed, where further jacking pushes the spudcan into the soil. In the presence of soft soils, spudcan foundations may require a penetration depth of up to 3 times the diameter of the spudcan to achieve a suitable bearing capacity for jack-up structures under large storm conditions (Hossain and Randolph, 2009). Once penetration ceases, the platform can be raised out of the water to the required height for operating conditions. Although linear trends of strength with respect to depth are often observed for uniform soils, complex layers can have profound impacts on the performance of spudcan (Li et al., 2016). As such, the variability of seabed strength and the associated effects on foundation performance remains the subject of considerable interest (Tang, 1979; Cheon and Gilbert, 2014; Li et al., 2017; Yi et al., 2020).

Guidelines suitable for calculating the bearing capacity of spudcans in sands, including Society of Naval Architects Marine Engineers (1991) and the International Organization for Standardization (2012) are based on conventional bearing capacity equations for shallow, flat circular footings, using empirical correlation factors to accommodate the differences between traditional footings and spudcan geometries. As such, these methods can produce inaccuracies due to the limitations in conventional bearing capacity theory involving dilatancy and compaction (Edwards et al., 2013). This is especially in the case where limited site investigation data is available, with parameters requiring estimate through soil correlations.(Hu et al., 2021). Furthermore, factors such as sand plugging beneath an advancing spudcan cannot be readily assessed through current ISO and SNAME guidelines (Teh et al., 2008). An overprediction of spudcan penetration depths in sandy soils was observed by Overy (2012), who suggested that laboratory tests are often required to determine suitable friction angles. Despite this recommendation, advanced laboratory test results are often unavailable for cases involving offshore jack-up installations. For both SNAME and ISO guidelines, the relative density andstress conditions of sandy deposits can impact the operative friction angle, although these factors are not explicitly accounted for in these guidelines (Osbone et al., 2009). As an alternative, in-situ Cone Penetrometer Tests (CPT) are suitable for inferring a wide range of soil properties through the measurement of both the shaft and cone end tip resistance (Schertmann, 1977). More recently, the use of Large Deformation Finite Element analysis (LDFE)

* Corresponding author.
E-mail address: ali.tolooiyan@utas.edu.au (A. Tolooiyan).

https://doi.org/10.1016/j.oceaneng.2023.114955
Received 22 August 2022; Received in revised form 12 May 2023; Accepted 27 May 2023
Available online 3 June 2023

has allowed for the simulation of CPT penetration responses, given the selection of a suitable constitutive model sufficient to describe the site conditions (Tolooiyan and Gavin, 2011; Chouhan and Chavda, 2023).

Large deformation numerical methods are increasingly prevalent in offshore computational geotechnics, providing a mechanism to evaluate the behaviour of soils at large strains (Randolph et al., 2005). A range of techniques allows for the simulation of large deformation soil behaviour in offshore environments, including Smoothed Particle Hydrodynamics (SPH) (Jin et al., 2019), the Material Point Method (Brinkgreve et al., 2017), the Remeshing and Interpolation Technique with Small Strains (RITSS) (Tian et al., 2014) and the Coupled Eulerian Lagrangian Method (CEL) (Wang et al., 2015). Wu et al. (2019) used SPH to consider soil-water-structure interaction through coupled analysis, while Hu et al. (2015) implemented CEL to describe the full load-penetration profile of mobile jack-up spudcan footings. Similarly, Arbitrary Lagrangian Eulerian method (ALE) simulations have been developed to model a range of processes related to the behaviour of spudcan structures in clay and sand (Nazem et al., 2009; Jiayu et al., 2018).

Initially defined by Noh (1963) under a two-dimensional framework for hydrodynamics simulations, ALE has proven a versatile model for a variety of large deformation geotechnical applications, ranging from slope stability analysis (Wang, 2014) to the pullout behaviour of embedded suction anchors (Na et al., 2014). Based on the operator split method first proposed by Benson (1989), ALE circumvents the drawbacks of mesh distortion associated with the traditional Lagrangian Finite Element Method formulation through the use of remeshing algorithms to update the Finite Element mesh distribution. Distortion is prevented through the decoupling of mesh and material displacements, introducing two sets of unknowns in the global equations (Nazem et al., 2009). Costes et al. (2017) noted that the quality of ALE results is dependent on the selection of an appropriate mesh updating algorithm.

Kellezi and Stromann (2003) and Kellezi et al. (2005) employed axisymmetric FEM analysis for modelling punch-through in layered soil due to jack-up spudcan penetration. In their analysis, different soil models were used for sand and clay, while model parameters were estimated from field and laboratory triaxial tests. Tho et al. (2012) conducted ALE FEM analyses in comparison with experimental results, noting that a sufficiently fine mesh is of paramount importance in obtaining accurate results, while the spudcan rate of penetration must be kept sufficiently slow to avoid dynamic effects impacting on the solution. The method was extended in addition work to consider spudcan-pile interactions (Tho et al., 2013). Kellezi et al. (2005) used 2D and 3D FEM analyses to assess the impact of the spudcan penetration on a neighbouring pipeline. They concluded that although the results of the 2D and 3D models were similar, 3D modelling is considered a beneficial approach to analyse the effect of spudcan penetration on neighbouring structures that do not exist strictly within a single plane. While each large deformation method displays a unique set of advantages and limitations based on the selected objective, ALE provides several salient features that are suitable for predicting spudcan penetration. CEL-based modelling accommodates extreme levels of deformation beyond what can be feasibly simulated using ALE. However, the method avoids the limitations associated with Eulerian penetration of the Lagrangian domain when geometric features are complex, as is commonly the case with spudcan geometries (Dassault Systèmes, 2022). As an ALE-based method, RITSS is a powerful large deformation tool using periodic remeshing to define a new mesh topology that is not influenced by the previous increment, tolerating strains beyond what is permissible with traditional ALE (Tian et al., 2014). Despite this useful feature, current implementations of RITSS require user-dependent computer codes which are not readily available in current commercial computer software.

This paper presents a mechanism for assessing spudcan load penetration behaviour in sandy deposits with limited available site investigation data through a procedure involving SPT soil correlations to perform a back-analysis of CPT penetration profiles, thereby determining relevant stiffness parameters with depth. The large deformation CPT models including the relevant soil stiffness parameters, are then used to develop large deformation spudcan models. This allows for large deformation Finite Element simulation of spudcans to be performed, with a simultaneous, multiple spudcan loading case presented. A case study consisting of numerical simulation and analysis using ALE was developed to consider the continuous penetration of a spudcan in variable sand deposits overlying shallow bedrock off the Tunisian coast, obtaining strong agreement with conventional methods. The proposed method of analysis is amenable to site conditions where minimal in-situ test results, geophysics or laboratory tests data are available. The technique compares analytic solutions with results from CPT back-analyses and large deformation simulations of spudcan penetration, providing a sound mechanism for the assessment of load penetration curves, as indicated by comparisons with relevant guidelines for shallow footings. Punch through failure at the test site was not deemed by the developers to be problematic, however the potential instability of the jack-up arising from scour beneath the foundation elements presented a concern. As a result, accurate prediction of the penetration was required to conduct an assessment of potential scour effects. Estimates of penetration were required to determine the moment fixity and foundation stiffness. These parameters were considered essential in assessing the structural integrity of the jack-up and whether there is adequate resistance against in-service loads over the operating 6-month lifetime, while an accurate determination of the spudcan penetration was complicated by the relatively sparse site investigation data available. This paper provides validation of results through comparative penetration analyses conducted using traditional shallow foundation methods.

2. Spudcan geometry and site conditions

The jack-up platform considered in this project consisted of a three-legged structure founded on conical spudcans installed in 10–20 m water depth, where the vertical platform load was 48 MN per spudcan. However, an additional preload was available to provide a margin of safety against operation loads, bringing the maximum installation load to 54 MN per spudcan. Each spudcan footing comprised a maximum cross-sectional diameter of approximately 14 m and a deflection angle θ, of 150° (Fig. 1).

Geotechnical investigations conducted at the site location consisted of a 200 mm diameter cable percussion borehole with sampling, followed by subsequent laboratory and in-situ testing. Continuous Standard Penetration Test (SPT) tests were performed with the blows recorded over 75 mm penetration intervals. Two continuous SPT *N* test profiles (signifying the number of blows per 300 mm) (Fig. 2) were performed to evaluate the in-situ density of the soils at the site, which

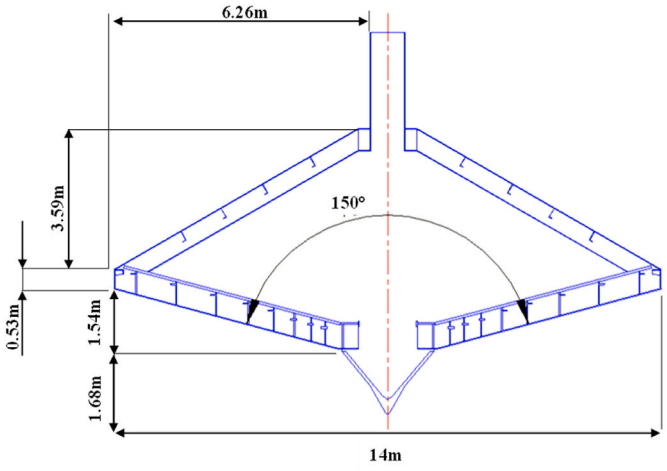

Fig. 1. Spudcan geometry.

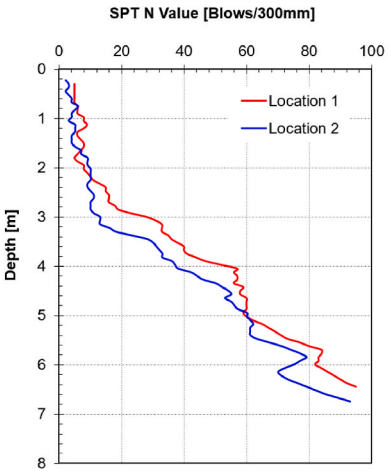

Depth (m)	Description	Classification	Legend
0 - 1	Loose light grey silty fine sand. Sand blowing back up casing to 3m above bed	Loose light grey silty fine sand	
1 - 2			
2 - 3	Sand becoming medium dense from 2m according to continuous SPT profiles obtained	Medium dense light grey silty fine sand	
3 - 4			
4 - 5	Sand becoming dense from 4m according to continuous SPT profiles obtained	Dense light grey silty fine sand	
5 - 6			
6 - 7			
7 - 8	Gravel/cobbles. Refusal, unable to advance below 7.5m	Gravel/cobbles, upper bedrock	

Fig. 2. Continuous SPT blow data and soil stratigraphy description.

were consistent across both locations. The measured SPT *N* values were considered as low (<10) for a depth of 2.2–3 m below bed level (*bbl*). Thereafter, the values increased significantly with depth, indicating that the deeper material is in a dense to very dense state. Notwithstanding the apparent similarity in the SPT *N* profiles, it is clear that the vertical boundary between the loose to medium dense sand and the underlying dense to very dense sand varied by approximately 0.4 m between the two boreholes, spaced approximately 40 m apart. As such, the observed variation indicates a mechanism whereby different spudcan penetrations can occur for the two site locations. Linear design profiles are assumed to describe the SPT variations with depth, with N increasing at a steeper rate in the dense sand below 3–4m compared to the overlying loose sand, as shown in Fig. 2, suggesting the presence of two layers, delineated at a depth of 3m bbl.

Tests conducted on disturbed soil samples revealed soils between 0 and ≈7.5 m *bbl* were grey silty fine sand with a mean particle size (D_{50}) of ≈0.42 mm. The continuous SPT tests and the borehole reached refusal between 6.53 and 7.5 m *bbl*, with a rotary core follow-on performed at the borehole location. Although recovery was very poor, the material was described as yellow-brown nodular, moderately strong to strong calcrete (caliche).

A geophysical report on the area identified the presence of an upper unit of weakly cemented fine to medium bioclastic sand between seabed level and 3.8 m *bbl*. This corresponds well with the zone with low SPT *N* values in Fig. 2. The geophysical report noted that lateral variations in this layer (due to differences in cementation) are likely to cause variations in the penetration during jack-up of the rig. The geological interpretation of the site suggests the sand is underlain by bedrock containing claystone, or sandstone and limestone beneath. No faulting or other geological features were identified with the soil and rock at this location. On this basis, the penetration resistance and stability of the spudcan foundations were performed using geotechnical parameters derived for the upper sand layers between 0 and 7.5 m *bbl*. Punch-through failure was not deemed to be a concern due to the presence of the dense sand underlying the loose upper sand layers and the relatively shallow bedrock.

The SPT profiles were used to determine the peak angle of friction (φ'_p) using a correlation proposed by Peck et al. (1953). The inferred

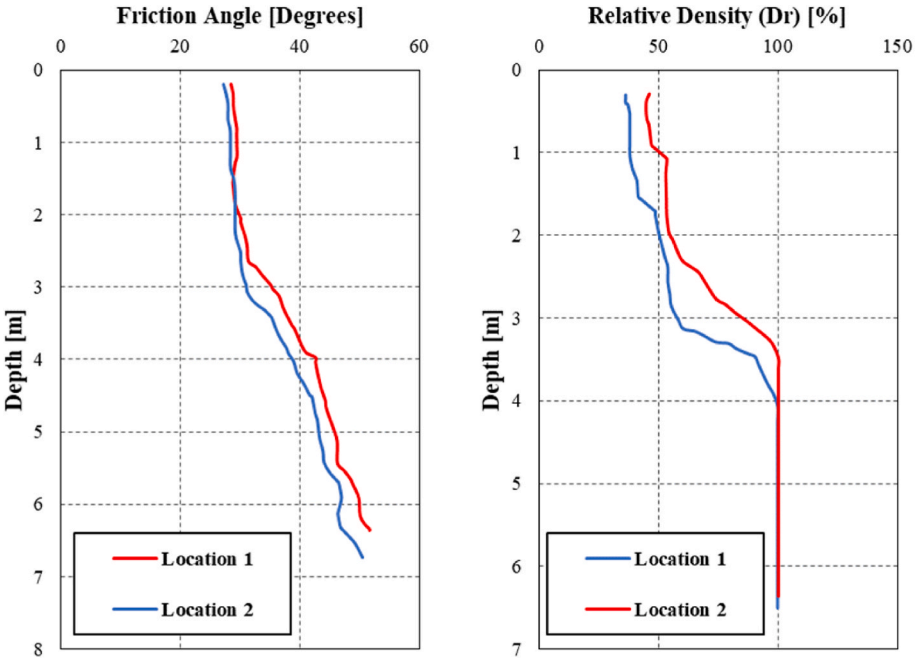

Fig. 3. Friction angle and soil density determined from SPT data.

friction angle, shown in Fig. 3, is seen to increase with depth from approximately 28° degrees at seabed level to 50° degrees at 6.8 m *bbl*, and it is relatively consistent between the SPT profiles. Friction angles measured in direct shear tests on samples obtained from 2 to 6 m *bbl* suggest the sand exhibited a φ' value greater than 37°. These values represent the peak friction angles of relatively dense samples.

The relative density was estimated using a correlation between $N1_{60}$ (where $N1_{60}$ is the SPT *N* value corrected for stress level effects) and D_r proposed by Skempton (1986). The D_r profile shown in Fig. 3 suggests the sand is medium dense to 3m *bbl* and dense to very dense below this depth. The Cone Penetration Test (CPT) q_c value can also be estimated using a correlation developed by Kulhawy and Mayne (1990), as shown in Equation 1

$$q_c = p_{atm} \times 5.44 \times N \times {D_{50}}^{0.26} \quad [1]$$

where, q_c is cone tip resistance; *N* is the number of SPT blows; D_{50} is the particle size of which 50% of the material is finer; and p_{atm} is the atmospheric pressure of 100 kPa. The CPT q_c profile (Fig. 4) was developed by substituting the measured SPT N values into Equation (1).

The high q_c value present in layer 2 is indicative of an overconsolidated deposit. A closed-form correlation to estimate the Overconsolidation Ratio (OCR) in sandy soils is recommended by Mayne (2005), as shown in Equation (2).

$$OCR = \left[\frac{0.192(q_t/p_{atm})^{0.22}}{(1-\sin\varphi')(\sigma'_v/p_{atm})^{0.31}}\right]^{\left(\frac{1}{\sin\varphi'-0.27}\right)} \quad [2]$$

Mayne (1995) also suggested closed-form correlations to estimate the ratio of in-situ horizontal to vertical stress (K_o), given by Equations (3) and (4). By varying the OCR, agreement can be achieved between Equations (3) and (4), with a reasonable profile of K_o determined.

$$K_o = 0.192\left(\frac{q_c}{P_a}\right)^{0.22} \times \left(\frac{\sigma_v'}{p_{atm}}\right)^{-0.31} \times OCR^{0.27} \quad [3]$$

$$K_o = (1-\sin\varphi')OCR^{\sin\varphi'} \quad [4]$$

Using either Equation (2) or the combination of Equations (3) and (4), the OCR value is estimated in the range between 10 and 11 for the dense sand layer below 3 m depth. The upper sand layer is assumed to be normally consolidated, and K_o is determined using Equation (4). The in-situ horizontal and vertical stress levels were estimated using this approach and are illustrated in Fig. 5.

3. Conventional penetration analysis

The predominant method for determining the penetration of spudcan footings in silica sand is given by the guidelines produced by the Society of Naval Architects Marine Engineers. The design method proposed by SNAME (2008) for determining the spudcan penetration is a direct application of conventional bearing capacity formulae for shallow circular flat footings. Empirical correction factors are introduced into the spudcan penetration analysis to account for the differences between conventional footings and penetrating spudcans. The vertical bearing capacity (F_v) of the penetrating spudcan is determined using the formula recommended by Hansen (1961) and reproduced as Equation (5).

$$F_v = A\left(0.5\gamma' BN_\gamma s_\gamma d_\gamma i_\gamma b_\gamma g_\gamma + qN_q s_q d_q i_q b_q g_q + cN_c s_c d_c i_c b_c g_c\right) \quad [5]$$

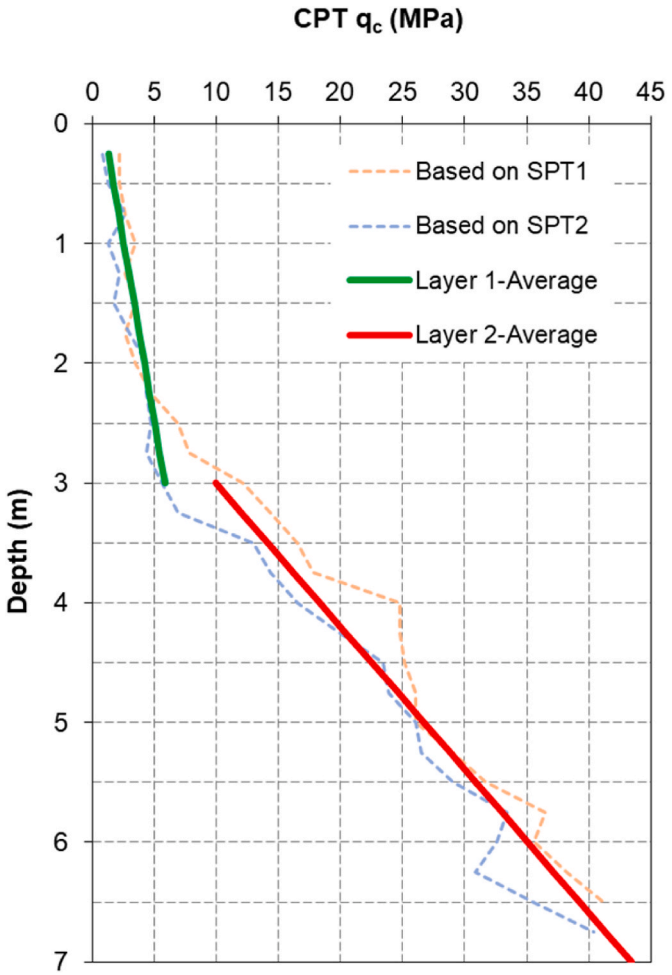

Fig. 4. Cone tip resistance estimated from correlation with SPT N values.

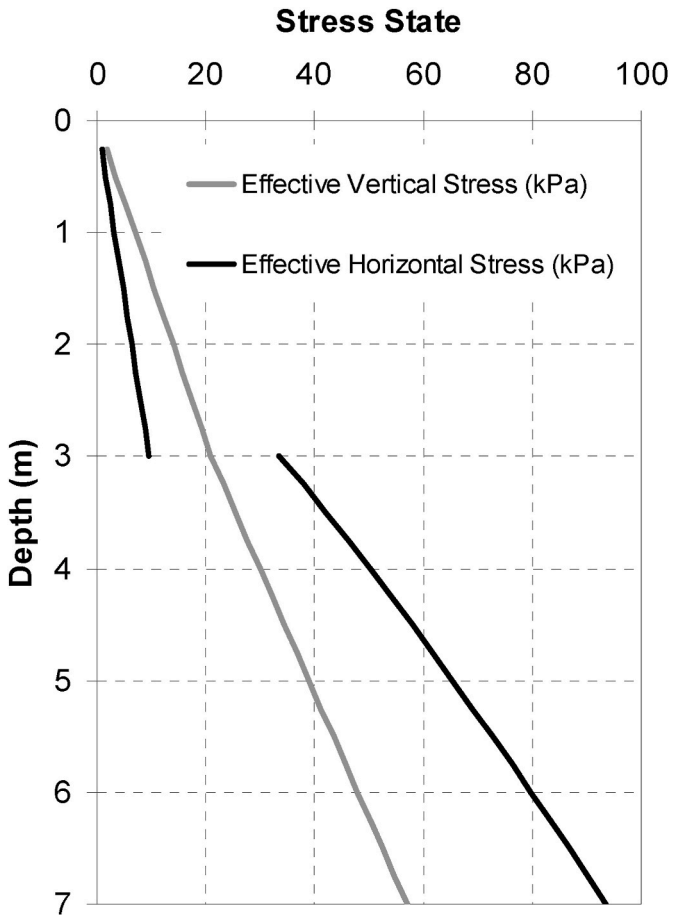

Fig. 5. The estimated horizontal and vertical stress level.

where, A is the cross-sectional area which is dependent on the effective spudcan diameter (D'), which refers to the spudcan diameter in direct contact with the soil; B is the foundation width; q is the vertical overburden; c is the cohesion; γ' is the effective soil unit weight; s_γ, s_q, s_c are the shape factors; N_γ, N_q, N_c are the bearing capacity factors; d_γ, d_q, d_c are the deapth factors; i_γ, i_q, i_c are the load inclination factors; b_γ, b_q, b_c are the base inclination factors; and g_γ, g_q, g_c are the ground inclination factors. However, the depth factor is equal to 1 until the maximum spudcan cross-section makes contact with the ground surface. The surcharge term in Equation (5) is equal to zero until the spudcan penetrates to sufficient depths that the maximum cross section is in direct contact with the soil. Therefore, the initial spudcan penetration simplifies to Equation (6). The friction angle incorporated in this analysis should be the operational friction angle controlling the soil failure around the penetrating spudcan and, therefore, may not be equal to the soil friction angle. Additional factors such as the foundation geometry should be taken into account in assessing an appropriate φ value.

$$F_V = A\left(0.5\gamma' B N_\gamma s_\gamma b_\gamma g_\gamma\right) \quad [6]$$

where, $N_\gamma = 1.5(N_q - 1)\tan\varphi$ and $N_q = e^{\pi \tan\varphi} \tan^2(45^\circ + \varphi/2)$. A revision to the SNAME guidelines (2008) identified three areas where spudcans are significantly different from conventional shallow foundations: (i) shape effects, (ii) loading type, and (iii) scale effects:

(i) Spudcans are conical and made from relatively smooth steel, whereas most shallow footings are rough concrete and flat.
(ii) Spudcan penetration analysis examines the foundation behaviour during installation rather than conventional loading and, therefore, must consider the large strains experienced by the soil.
(iii) Scale effects must be considered as most spudcans are an order of magnitude larger than conventional footings.

The issues identified by the SNAME (2008) revision document have been used to explain field observations from jack-up installations in the North Sea, which underwent significantly larger penetrations than those predicted using traditional bearing capacity factors determined from the measured triaxial data (with friction angles in the range from 30 to 40°). To determine appropriate design soil parameters and bearing capacity factors, the SNAME guidelines recommend reducing the measured friction angles from triaxial tests by 5° to predict the penetration of footings in silica sand. Various studies have observed that reduced friction angles should be used as a correction for scale effects (Graham and Stuart, 1971; James and Tanaka, 1984; Kimura et al., 1985). In the absence of triaxial test data, the default design values presented in Table 1 can be selected based on the soil density. It is worth noting that the friction angles given in Table 1 are not direct material parameters but are design friction angles and design values, which are meant to account for the scale, loading, and shape effects.

Table 1
Design parameters for cohesionless silica soil (Society of Naval Architects Marine Engineers, 2008).

Density	Soil Description	φ Design (°)	N_γ	N_q
Very Loose	Sand	15	2.6	3.9
Loose	Sand-Silt			
Medium	Silt			
Loose	Sand	20	5.4	6.4
Medium	Sand-Silt			
Dense	Silt			
Medium	Sand	25	11	11
Dense	Sand-Silt			
Dense	Sand	30	22	18
Very Dense	Sand-Silt			
Dense	Gravel	35	48	33
Very Dense	Sand			

In the absence of high-quality triaxial test data for this site, design bearing capacity factors were determined from Table 1, using relative densities derived from the SPT N values. The resulting spudcan penetration curves were seen to increase with depth, reflecting the increase in relative density and the increasing effective diameter. The maximum preload available to aid the installation process was 54 MN, resulting in a predicted design penetration of 2.4 m (See Fig. 6) as per Equation (6).

Model tests conducted by De Beer (1965) and more recently by Zhu et al. (2001) identified a scale effect with the bearing capacity factor, N_γ, reducing with increasing foundation width. This is thought to be due to the increasing foundation geometry mobilising a deeper and larger volume of soil with a higher mean stress. The dilatancy component of the soil reduces as the mean stress increases, and N_γ is, therefore, inversely related to the footing diameter. As a result, the normalised bearing pressure for the large spudcan geometries should be lower than observed with traditional design methods. White et al. (2008) used model centrifuge tests to examine the impact of the scale effect in conjunction with the conical foundation shape and determined that the back calculated bearing capacity factors for conical spudcans were a factor of 2 lower than flat footings in dense sand. This was attributed to a progressive failure mechanism that developed due to the pre-shearing effect of the penetrating point of the spudcan, causing local failure and preventing the peak resistance being mobilised simultaneously over the entire failure plane. Theoretical pairs of friction angles and bearing capacity factors were provided by White et al. (2008), which for large foundations in dense sand show reasonable agreement with the SNAME guidelines and result in a penetration depth of 2.6 m for the spudcan subjected to the ultimate preload of 54 MN. As the spudcan diameter and relative density decrease, the SNAME bearing resistance and the theoretical predictions compared with White et al. (2008) deviate significantly, predicting much higher installation resistance and hence lower penetrations. Although limited experimental support was provided by White et al. (2008) to support these findings for loose to medium dense

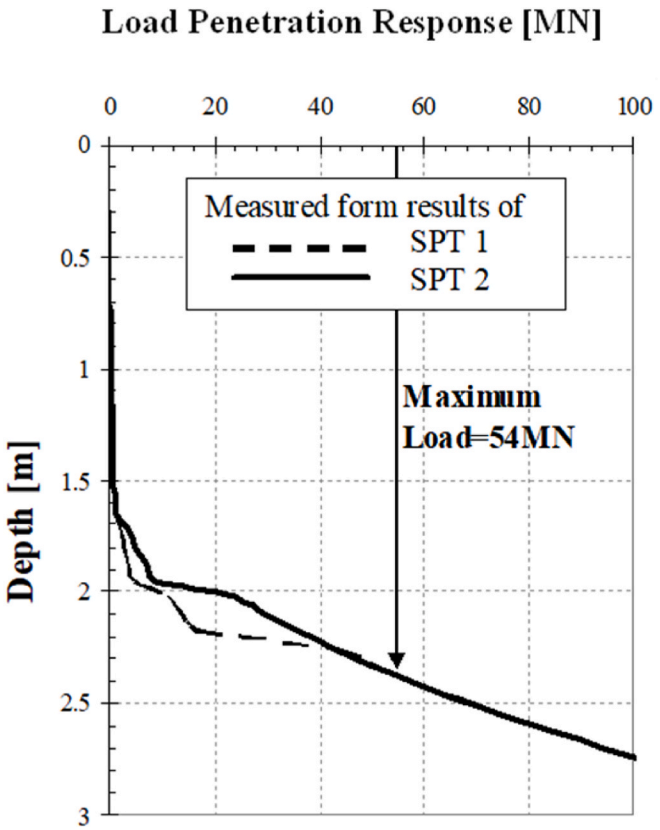

Fig. 6. Conventional penetration curve via Equation (6) (Hansen, 1961).

sand, while excellent agreement was achieved between the penetration depths determined by the SNAME (2008) and White et al. (2008) approaches for this site, this may not necessarily hold for sites of lower relative densities.

4. Numerical investigation

In this paper a penetration study was performed using an ALE FEM model, which was implemented in a large strain *Abaqus/Explicit* code. Considering the importance of penetration depth in determining the spudcan stiffness and moment fixity and in light of the issues surrounding scale and geometry effects, the spudcan penetration was deemed worthy of a more detailed analysis using advanced Finite Element Method (FEM) approaches. As opposed to the aforementioned conventional analysis presented, soil profiles were determined directly from CPT simulations, with the resulting layering used in the spudcan penetration models to follow. As such, the simulation process involved three stages: (i) model calibration (ii) 2D axisymmetric analysis and (iii) 3D analysis of the footing penetration. A schematic of the proposed method of analysis combining field test data, SPT-soil correlations, ALE CPT and spudcan simulations and conventional bearing capacity guidelines is presented in Fig. 7.

4.1. Finite Element formulation

Benson (1989) proposed an "operator split" method for ALE, allowing mesh displacements and material displacements to be decoupled through a two-step analysis process, consisting of an Updated Lagrangian step (UL) and an Eulerian step. In the ALE method, mesh displacements are separate from the material displacements and are considered as arbitrary, hence the name. In the Euler step, a new adaptive mesh is generated from the deformed domain with all state variables transferred from the old to the new mesh. Remapping is considered at Gauss (integration) points for components such as stress and nodal points for displacements, velocities and accelerations using a first-order Taylor series expansion with the basic ALE kinetic energy formula (Benson, 1989)

$$\dot{f}^r = \dot{f} + \left(v_i - v_i^r\right)\frac{\partial f}{\partial x_i} \quad [7]$$

where, $\dot{f}^r$ and $\dot{f}$ are the time derivatives of functions applied to mesh and material coordinates, respectively; v_i and v_i^r are the material and mesh velocities, respectively, with their difference known as the convective velocity; and x_i are the system coordinates. A procedure for remapping integration point variables for geotechnical applications is given by Nazem et al. (2006).

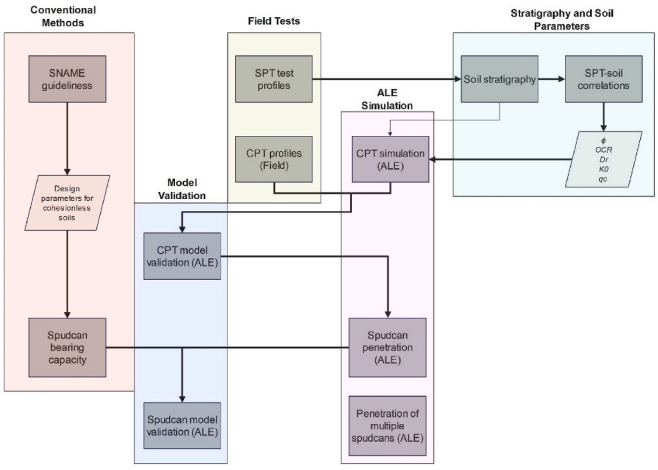

Fig. 7. Schematic of the proposed simulation methodology.

4.2. Model calibration

A 2D axisymmetric Finite Element Analysis was performed using *Abaqus/Explicit* to simulate the penetration of spudcans in a layer of sand 7 m in depth. The first step of the FEM analysis involved estimating the soil parameters required for calibration of the constitutive soil model (Drucker Prager which is suitable for simulating the elastic-plastic behaviour of loose granular materials such as sands in *Abaqus/Explicit* with high computational efficiency compared with alternative models e. g. Mohr-Coulomb). For the FEM simulation of this case history, the primary site investigation results consisted of 2 SPT profiles. This data was used to indirectly calibrate the FEM soil model by first simulating a Cone Penetration Test (CPT) using *Abaqus/Explicit*.

The CPT is widely used for offshore foundation design and is a useful tool for calibrating soil models in FEM. Tolooiyan and Gavin (2011) describe a method of generating CPT q_c profiles by using a large strain adaptive meshing technique. This method was used herein to generate synthetic CPT profiles, which could be compared to the q_c profiles previously estimated using well-known correlations with SPT N values. Simple assumptions were made for the initial vertical stress state of the sand layer. The unit weight of sand (γ) was considered to be 17 kN/m^3 and 19 kN/m^3 for the loose and dense layers, respectively, with $D_{50} =$ 0.42. A critical state friction angle of 33° was also assumed, which is applicable for large deformation analyses where strength parameters are post-peak. Pure master-slave kinematic tangential contact definitions were given for both the cone-soil and shaft-soil contacts, with a friction coefficient equal to 0.334 – signifying the friction between steel and sand (Tolooiyan and Gavin, 2011). Due to large displacements, the master surface tracks the slave surface nodes via a contact tracking algorithm (Dassault Systèmes, 2022). The lateral stresses used in the FEM model were assumed to equal the values estimated from the SPT/CPT correlations previously presented in Fig. 5. The CPT q_c is a function of sand stiffness, friction angle, OCR and in-situ stress state. However, all parameters have been estimated except the sand stiffness. The sand stiffness was determined by back-analysis interpreted by CPT profiles produced within a FEM model. In this FEM analysis, sand is modelled as a linear elastic perfect plastic material while the linear stiffness is a function of in-situ stress level. An initial stiffness value was assumed, and a CPT profile was generated. This process was iterated with different stiffness values until good agreement was achieved between the simulated CPT resistance and the q_c profile estimated from the SPT.

Due to the large number of elements required to model the installation of a 36 mm penetrometer to such a relatively large depth, and the consequent significant computational time required, the actual soil cluster considered in the analysis is 1500 mm wide and 3000 mm deep. Multiple analyses for different depth intervals were performed where the vertical overburden stress over the soil cluster was changed (at a rate of 7 and 9 kPa per metre for the top and bottom soil clusters, respectively). The soil within each cluster was assumed to be weightless to give a constant initial vertical stress over the entire penetration depth, which allowed the q_c value to be related back to a specific depth within the main soil strata.

An axisymmetric model, which included 35946 CAX4R elements and 36244 nodes, is presented (Fig. 8). The boundaries were modelled using CINAX4 4-node linear, one-way infinite elements. The use of infinite elements minimizes the effects of the boundary conditions, inhibiting reflected energy from impacting the region of interest, without the requirement of a prohibitively large modelling domain. In this case, infinite elements were implemented along the bottom and right-hand boundaries of the model geometry. The 18 mm radius cone, with a cone angle of 60° and CPT body was modelled using two independent analytical rigid surfaces, which allowed the cone tip stresses to be separated from friction developed along the cone sleeve. The friction at the cone-soil interface is assumed to be 50 percent of the soil-soil friction

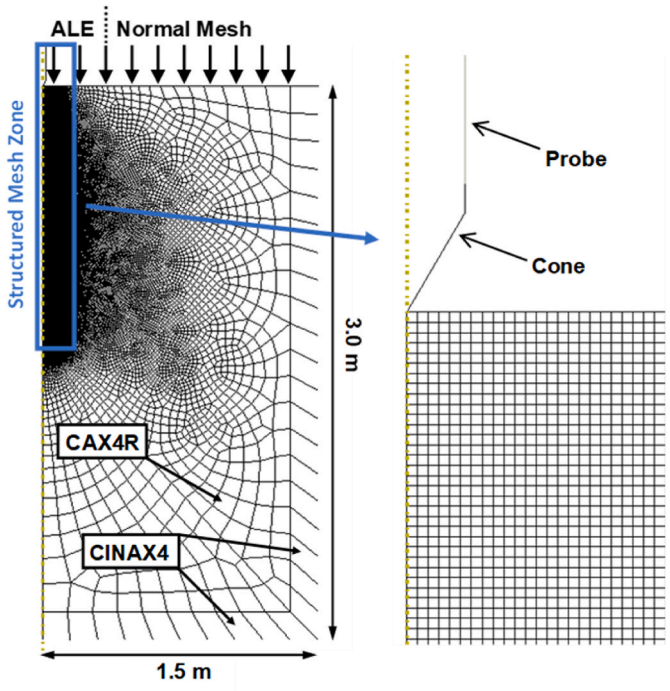

Fig. 8. Geometry of the CPT Finite Element Method simulation.

to account for the smooth steel cone material. Cone penetration starts from the top surface and continues to 1.5m depth. During penetration, the q_c value increases with depth and finally reaches a steady state level which is the CPT q_c value in the modelled depth. An ALE remeshing algorithm was used to cope with the large strains directly adjacent to the penetrating cone tip (Fig. 8). The model contained a structured mesh surrounding the penetration zone with a horizontal dimension approximately 3 times the size of the CPT cone radius, with an unstructured mesh extending thereafter to the model boundaries. The use of both structured and unstructured mesh regions allowed for improved resolution of regions surrounding the CPT probe where large deformation takes place, and a coarser mesh in regions at a distance from the CPT insertion. Fig. 9 shows the analysis of the CPT value at a stress level equal to 0.5, 4.5, and 6.5 m depth below the seabed level The load settlement response was considered over a series of 1-m depth intervals, with the associated q_c profiles representing the penetration of the cone over 1500 mm from the commencement of each individualsimulation.

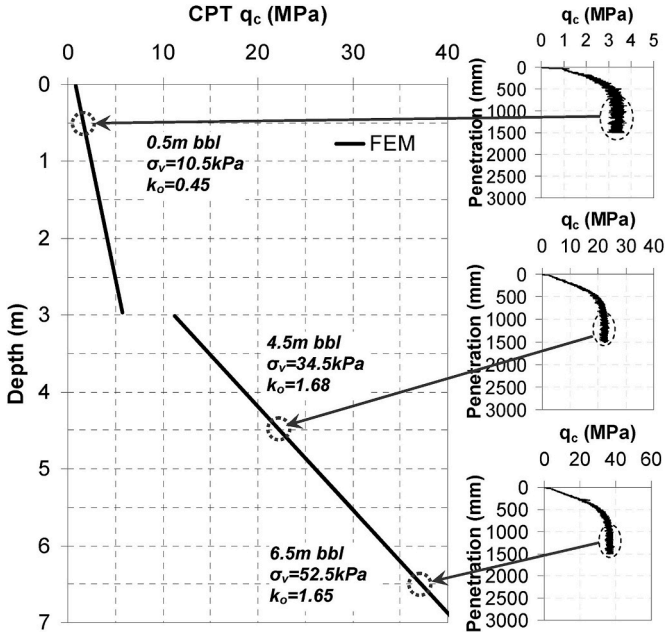

Fig. 9. Simulation of CPT q_c value in 0.5m, 4.5m and 6.5m depth below seabed level.

Trial efforts for choosing the appropriate stiffness values (E) of the sand showed excellent agreement between the correlated q_c and FEM q_c profiles when $E = 9q_c$, as shown in Fig. 10. Strong agreement is observed for depths below 3 m, while it is perhaps possible to obtain greater accuracy by further sectioning the soil domain into smaller sub-sections at greater depths, thereby allowing for even more accurate selections of the chosen stiffness values. The soil model used for the CPT simulation provided a calibrated soil model that can be used for performing the spudcan penetration analysis at this site. The subsequent FEM analysis of the spudcan adopts identical soil parameters as for the CPT modelling, including the aforementioned stress states, OCR, friction angle and the sand stiffness value equal to $9q_c$.

4.3. 2D axisymmetric analysis of single spudcan

Simulation of spudcan penetration was modelled in a similar manner to that of the CPT results presented in Section 4.2. In this analysis, an ALE re-meshing technique was employed in the region surrounding the penetration zone to avoid excessive mesh distortion (Fig. 11). The left boundary is an axis of symmetry permitting only positive radial displacements. The bottom boundary is fixed against horizontal and vertical displacement at 7 m depth to account for the relatively shallow bedrock. The right boundary is 100 m from the axis of symmetry and is fixed against horizontal displacement. The spudcan is modelled using an

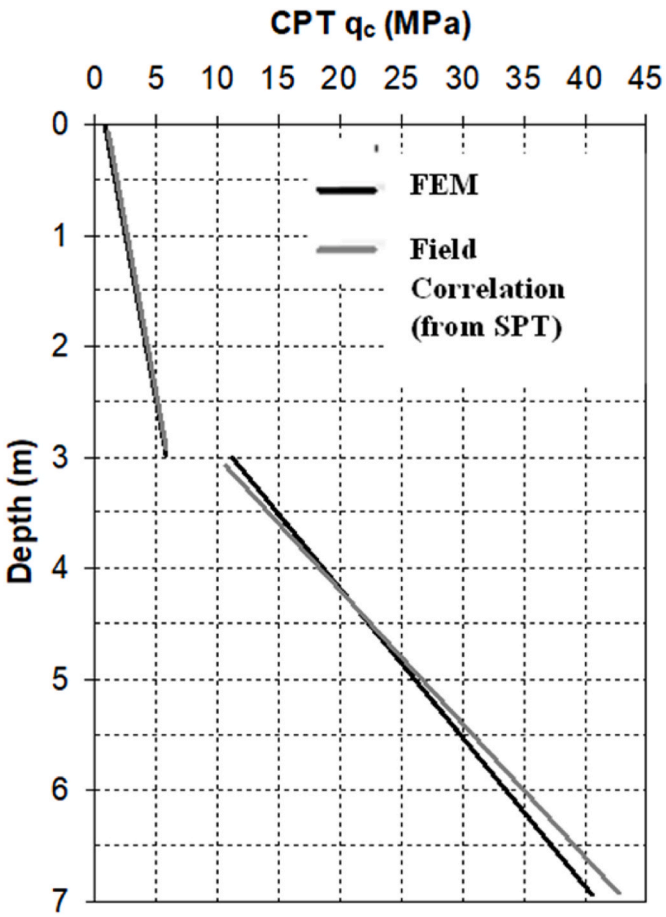

Fig. 10. Comparison between measured q_c profile and FEM q_c profile.

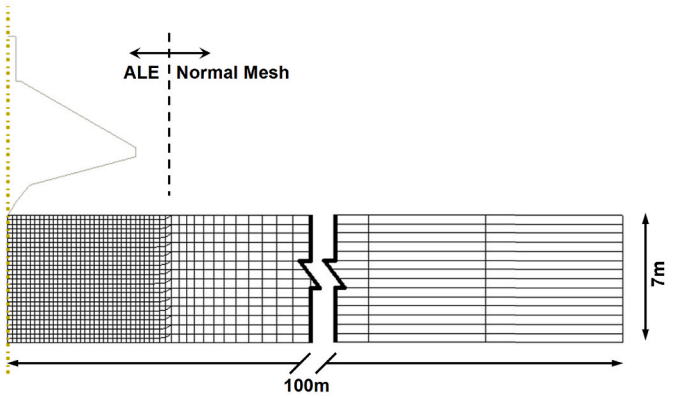

Fig. 11. Designed geometry for FEM analysis of spudcan penetration in axisymmetric condition.

analytical rigid surface, and the soil cluster is modelled using 1498 CAX4R elements. The soil-spudcan interface friction was assumed to be 50 percent of the soil-soil friction to account for the smooth steel surface of the spudcan.

The spudcan was gradually loaded until the load reached the maximum available preload of 54 MN. The load-penetration curve is shown in Fig. 12, where the maximum penetration was determined to be 2.61 m. The resulting spudcan behaviour compared with original analytical predictions based on Equation (6) (as presented in Fig. 12) shows excellent agreement, adding confidence in the initial design process. At a depth of 2.5 m, differences between the conventional results (Equation (6)) and large deformation Finite Element load penetration can be observed. The complex stress-strain behaviour of the simulated spudcan penetration is attributed to the differences in load penetration, whereby soil deformation profiles can include complex rotation and lateral displacement, as indicated in Fig. 13.

Soil deformation around the penetrated spudcan is shown in Fig. 13, indicating that in the region directly below the spudcan, both horizontal and vertical deformations are evident. However, remote from the axis of symmetry, the displacement trend becomes fully horizontal. This displacement pattern is due to the relatively shallow rock, and the constrained bottom boundary, where the soil does not have enough room for vertical displacement and the soil is forced to move laterally away from the axis of symmetry. This could have significant implications if the jack-up rig is installed in areas near to sensitive marine structures, such as offshore oil and gas facilities. In this instance, the lateral soil displacements could generate an additional loading component on the adjacent structure. The horizontal displacement pattern also indicates that the value of the initial horizontal stress is an important parameter influencing the design. The level of horizontal stress after the spudcan is installed is shown in Fig. 14.

The maximum horizontal stress at a distance of 50m from the centre of the penetrated spudcan is 152 kPa. This value is significantly higher than the initial horizontal stress at this location of 65–90 kPa, indicating that despite the 50m lateral soil extent there is still a small boundary effect. This is particularly interesting, considering that the distances between the legs of the jack-up unit are less than 45m (Fig. 15), and as a result, the three penetrating spudcans may have an influence on each other. Due to high-stress level in the vicinity of neighbouring spudcans, three-dimensional analyses are required to model the effect of one spudcan penetration on the penetration of a neighbouring spudcan.

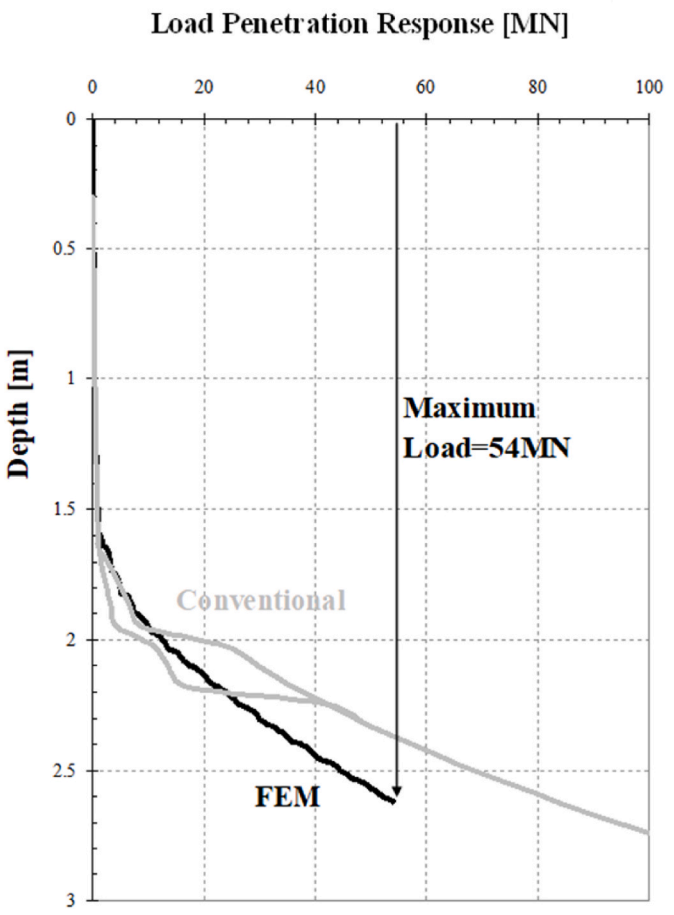

Fig. 12. Result of FEM analysis of spudcan penetration in axisymmetric condition compared with conventional analysis – Equation (6) (Hansen, 1961),

4.4. 3D analysis of three spudcans

3D modelling of spudcan penetration was also performed using Abaqus/Explicit, with a geometry consisting of 197,260 C3D8R elements presented in Fig. 16. The bottom boundary surface is fixed against any displacement, and as shown in Fig. 17, the side boundaries are placed over 100 m from each spudcan and are fixed against horizontal displacement. The ALE re-meshing technique was applied on elements around and below the spudcans, while the three spudcans SC1, SC2 and SC3 were modelled using analytical rigid surfaces. The same soil model and parameters were used as for the 2D analysis.

Spudcan penetrations were performed based on two different scenarios and two separate analyses.

Scenario I: Spudcan SC1 was loaded up to 54 MN, spudcan SC2 loaded after penetration of SC1, and subsequently SC3 loaded after penetration of SC2.

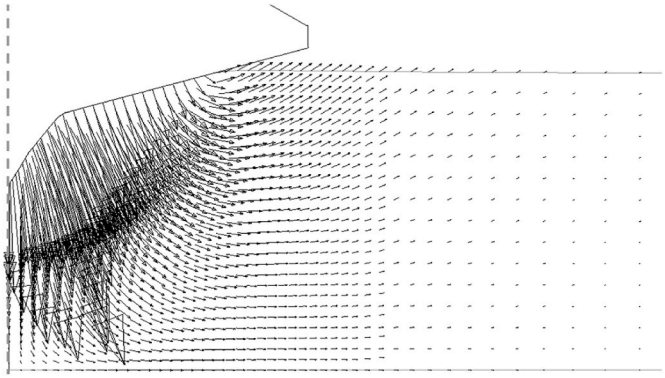

Fig. 13. Soil displacement below the penetrated spudcan.

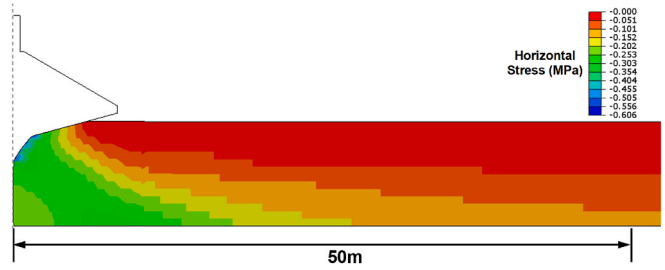

Fig. 14. Horizontal stress level around the penetrated spudcan.

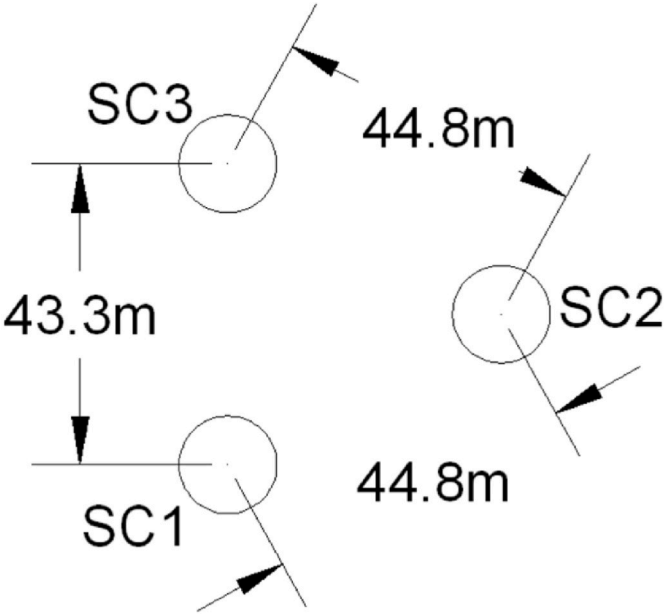

Fig. 15. Schematic of the distance between spudcans.

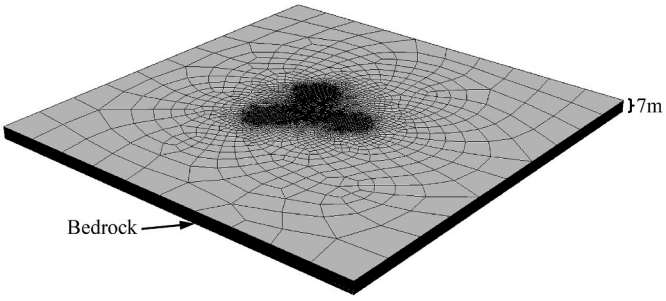

Fig. 16. Mesh distribution of the 3D model.

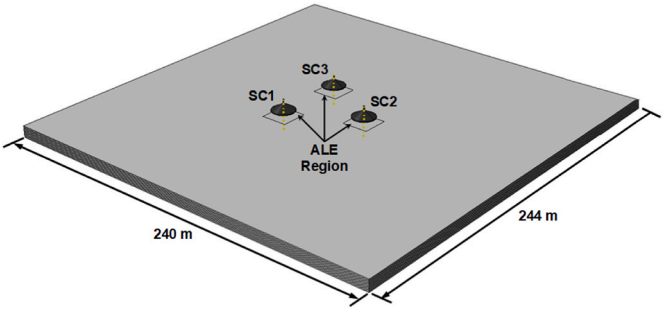

Fig. 17. Model geometry and dimensions.

Scenario II: All spudcans were loaded together up to 54 MN, penetrating the soil simultaneously.

Fig. 18a shows the load-penetration curves of the spudcans for *Scenario I* where each spudcan is loaded separately. In this analysis, SC1 and SC2 have very similar penetration curves, with both penetrating to 2.59 m depth. However, SC3 penetrated 1.4% less than SC1, indicating a small influence from the previously installed spudcans. To investigate the sensitivity of penetration depth of SC3 to the distance between spudcans, the structures were placed 22 m further away from each other in a separate analysis, with SC3 penetrating 2.8% less than SC1 (Fig. 18b). The difference between the maximum penetration value of SC3 and the other spudcans is due to stress accumulation below SC3 as a result of the penetration of SC1 and SC2. The increase in horizontal stress is illustrated in Fig. 19a, which shows the horizontal stress level ranging from 77 to 154 kPa below the SC3 footing before its penetration. These values are 70% higher than the initial horizontal stresses reflecting the influence of SC1 and SC2. Fig. 18b shows the lateral displacement of soil after penetration of SC1, which describes the failure mode below the spudcan.

In the second loading scenario, all three spudcans were loaded simultaneously up to 54 MN each. Load-penetration curves of the three spudcans in this analysis are shown in Fig. 20, highlighting a uniform stress distribution below all three spudcans and an identical load-penetration curve, which is estimated while the maximum penetration depth is 2.58 m.

5. Conclusion

In this research, the load penetration response of a spudcan footing in sand overlying bedrock was analysed using a conventional load-displacement approach, while a more sophisticated advanced Arbitrary Lagrangian Eulerian technique was presented to model penetration behaviour with large deformation simulation for use in the presence of limited site investigation data. Results were obtained by defining a process involving well-known soil and SPT correlations to perform a back-analysis of CPT penetration using large deformation Finite Element methods which were further used to develop large deformation spudcan penetration models.

The proposed method of analysis for considering spudcan penetration behaviour in loose sandy soils involved the following salient procedural steps.

(1) Use of well-known soil and SPT correlations to determine the necessary parameters for numerical simulation for use when limited soil data availability.
(2) Back analyses of axisymmetric CPT profiles to obtain relevant depth-dependent stiffness parameters to develop further large deformation spudcan penetration models.
(3) Creation of large deformation spudcan simulations which can be used to simulate complex stress conditions involving multiple spudcan footings (in three dimensions).
(4) Description of lateral stresses induced by penetration of a single spudcan; and simultaneous penetration of multiple spudcans, with an assessment of the impact on neighbouring spudcan behaviour.

Excellent agreement was achieved between the results of the conventional load-displacement approach and the proposed method incorporating SPT-soil correlations, CPT back-analyses and ALE spudcan simulation. As a result, the method demonstrates an alternative to methods given through SNAME guidelines (which, in some cases, may result in an overprediction of bearing capacities due to assumptions based on the selection of appropriate soil parameters and spudcan geometries).

The results presented in the case study of this research, highlight the

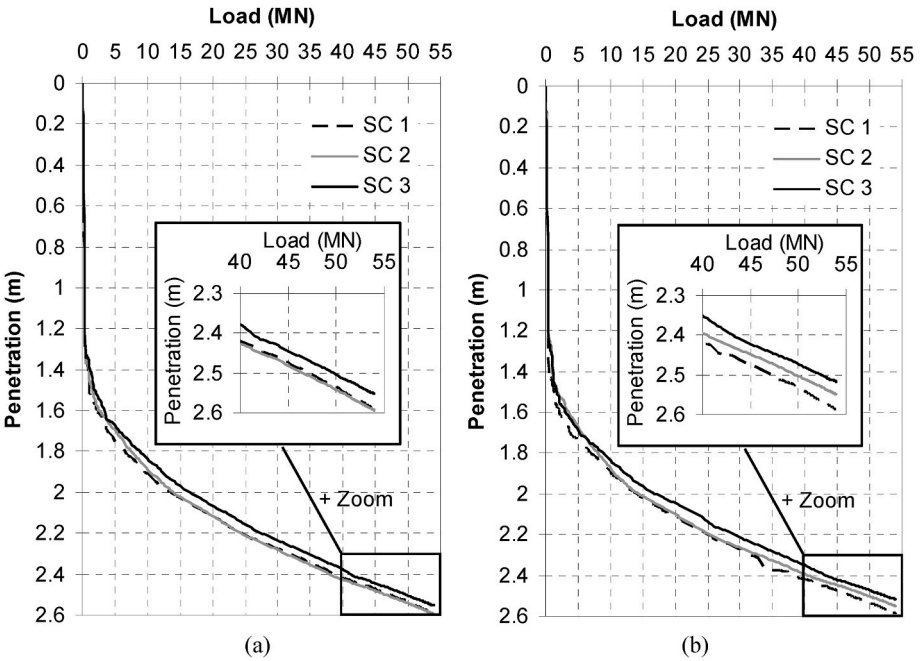

Fig. 18. Load-penetration curves when spudcans were loaded separately, (a) 44 m distance between spudcans, (b) 22 m distance between spudcans.

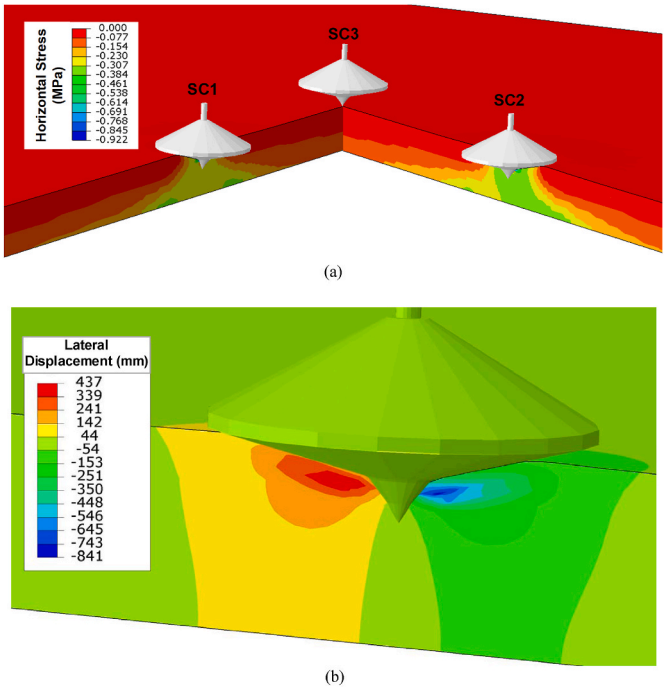

Fig. 19. (a) Horizontal stress below the SC3 after penetration of SC1 and SC2, (b) Lateral displacement of soil below the SC1 before penetration of SC2.

applicability of the Arbitrary Lagrangian Eulerian method as a mechanism to assess spudcan penetration in both 2D and 3D, particularly when the interactions of various loading regimes must be assessed. As an advanced numerical method for large strain simulation, the observed behaviour constitutes a sound method for simulating spudcan load penetration when calibrating behaviour based on limited geotechnical site investigation data and laboratory tests, as demonstrated through a case study involving a loose to medium dense sand overlying a dense to very dense sand.

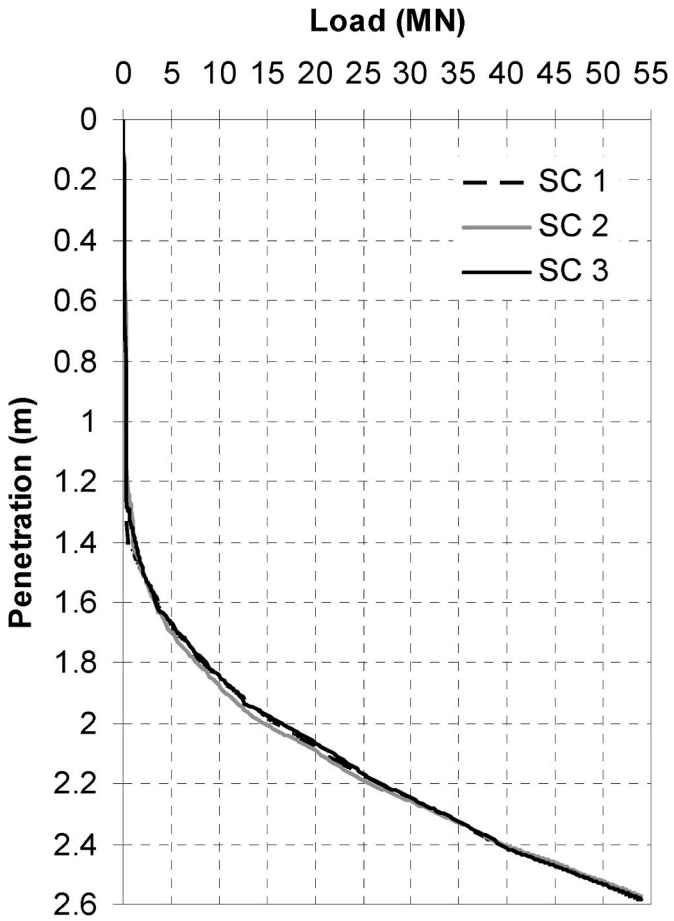

Fig. 20. Load-penetration curves when all 3 spudcans penetrate simultaneously.

Availability of data and material

Specific data can be provided on request by the corresponding author.

CRediT authorship contribution statement

Ali Tolooiyan: Conceptualization, Methodology, Study design, Software, Validation, Formal analysis, Investigation, Data curation, Writing – original draft, Visualization, Project administration. **Kenneth Gavin:** Conceptualization, Methodology, Study design, Software, Investigation, Resources, Writing – review & editing, Supervision, Project administration, Funding acquisition. **Ashley P. Dyson:** Conceptualization, Validation, Investigation, Writing – original draft, Visualization.

Declaration of competing interest

The authors declare that they have no known competing financial interests or personal relationships that could have appeared to influence the work reported in this paper.

Data availability

Data will be made available on request.

References

Benson, D.J., 1989. An efficient, accurate, simple ale method for nonlinear finite element programs. Comput. Methods Appl. Mech. Eng. 72 (3), 305–350.

Brinkgreve, R., Burg, M., Liim, L.J., Andreykiv, A., 2017. On the practical use of the Material Point Method for offshore geotechnical applications. Proceedings of the 19th ICSMGE.

Cheon, J., Gilbert, R., 2014. Modeling spatial variability in offshore geotechnical properties for reliability-based foundation design. Struct. Saf. 49, 18–26.

Chouhan, K., Chavda, J.T., 2023. A novel approach to simulate cone penetration test using conventional FEM. Geotech. Geol. Eng. 41 (2), 1439–1451.

Costes, J., Ghidaglia, J.M., Breil, J., 2017. Mesh regularization for an ALE code based on the limitation of the Lagrangian mesh velocity. Int. J. Numer. Methods Fluid. 85 (10), 599–615.

Dassault Systèmes, 2022. ABAQUS/Explicit 2022. Vélizy-Villacoublay, France [Computer software].

De Beer, E., 1965. Bearing Capacity and Settlement of Shallow Foundations on Sand. Proc. Symp. Bearing capacity and settlement of foundations, Duke University.

Deng, W., Tian, X., Han, X., Liu, G., Xie, Y., Li, Z., 2021. Topology optimization of jack-up offshore platform leg structure. Proc. IME M J. Eng. Marit. Environ. 235 (1), 165–175.

Edwards, D., Bienen, B., Pucker, T., Henke, S., 2013. Evaluation of the Performance of a CPT-Based Correlation to Predict Spudcan Penetration Using Field Data. 14th Int. Conf. The Jack-Up Platform–Design, Construction & Operation.

Graham, J., Stuart, J.G., 1971. Scale and boundary effects in foundation analysis. J. Soil Mech. Found Div. 97 (11), 1533–1548.

Hansen, J.B., 1961. The ultimate resistance of rigid piles against transversal forces. Bulletin 12, 1–9. Danish Geotech. Institute.

Hossain, M.S., Randolph, M.F., 2009. New mechanism-based design approach for spudcan foundations on single layer clay. J. Geotech. Geoenviron. Eng. 135 (9), 1264–1274.

Hu, P., Haghighi, A., Coronado, J., Leo, C., Liyanapathirana, S., Li, Z., 2021. A comparison of jack-up spudcan penetration predictions and recorded field data. Appl. Ocean Res. 112, 102713.

Hu, P., Wang, D., Stanier, S.A., Cassidy, M.J., 2015. Assessing the punch-through hazard of a spudcan on sand overlying clay. Geotechnique 65 (11), 883–896.

International Organization for Standardization, 2012. Petroleum and Natural Gas Industries: Site-specific Assessment of Mobile Offshore Units. Jack-ups Commentary and Detailed Sample Calculation, ISO.

James, R., Tanaka, H., 1984. An Investigation of the Bearing Capacity of Footings under Eccentric and Inclined Loading on Sand in a Geotechnical Centrifuge.

Jiayu, W., Run, L., Chao, L., Hui, X., Jun, W., 2018. Study on ALE Method for Simulating Spudcan Penetrating Near Piles. International Conference on Offshore Mechanics and Arctic Engineering, American Society of Mechanical Engineers.

Jin, Z., Yin, Z.-Y., Kotronis, P., Jin, Y.-F., 2019. Numerical investigation on evolving failure of caisson foundation in sand using the combined Lagrangian-SPH method. Mar. Georesour. Geotechnol. 37 (1), 23–35.

Kellezi, L., Kudsk, G., Hansen, P., 2005. FE modelling of spudcan–pipeline interaction. Proc. ISFOG 551–557.

Kellezi, L., Stromann, H., 2003. FEM Analysis of Jack-Up Spudcan Penetration for Multi-Layered Critical Soil Conditions. BGA International Conference on Foundations: Innovations, observations, design and practice: Proceedings of the international conference organised by British Geotechnical Association and held in Dundee, Scotland on 2–5th September 2003, Thomas Telford Publishing.

Kimura, T., Kusakabe, O., Saitoh, K., 1985. Geotechnical model tests of bearing capacity problems in a centrifuge. Geotechnique 35 (1), 33–45.

Kulhawy, F.H., Mayne, P.W., 1990. Manual on Estimating Soil Properties for Foundation Design - Report Number EL-6800. Electric Power Research Inst, Palo Alto, CA (USA). https://www.osti.gov/biblio/6653074 (Cornell Univ., Ithaca).

Li, J., Zhou, Y., Zhang, L., Tian, Y., Cassidy, M.J., Zhang, L., 2016. Random finite element method for spudcan foundations in spatially variable soils. Eng. Geol. 205, 146–155.

Li, L., Li, J., Huang, J., Liu, H., Cassidy, M.J., 2017. The bearing capacity of spudcan foundations under combined loading in spatially variable soils. Eng. Geol. 227, 139–148.

Mayne, P., 1995. CPT Determination of OCR and Ko in Clean Quartz Sands. Symposium on Cone Penetration Testing.

Mayne, P., 2005. Integrated Ground Behavior: In-Situ and Labs Tests. Deformation Characteristics of Geomaterials. CRC Press, pp. 162–185.

Na, S.H., Jang, I.S., Kwon, O.S., Lee, S.H., 2014. Study on pullout behavior of embedded suction anchors in sand using ALE (Arbitrary Lagrangian Eulerian) Technique. KSCE J. Civil Environ. Eng. Res. 34 (1), 167–173.

Nazem, M., Carter, J.P., Airey, D.W., 2009. Arbitrary Lagrangian–Eulerian method for dynamic analysis of geotechnical problems. Comput. Geotech. 36 (4), 549–557.

Nazem, M., Sheng, D., Carter, J.P., 2006. Stress integration and mesh refinement for large deformation in geomechanics. Int. J. Numer. Methods Eng. 65 (7), 1002–1027.

Noh, W.F., 1963. CEL: A Time-dependent, Two-Space-Dimensional, Coupled Eulerian-Lagrange Code, Lawrence Radiation Lab. Univ. of California, Livermore.

Osbone, J., Houlsby, G., Teh, K., Leung, C., Bienen, B., Cassidy, M., Randolph, M., 2009. Improved Guidelines for the Prediction of Geotechnical Performance of Spudcan Foundations during Installation and Removal of Jack-Up Units. Improved guidelines for the prediction of geotechnical performance of spudcan foundations during installation and removal of jack-up units, Offshore Technology Conference.

Overy, R., 2012. Predicting Spudcan Penetration in Loose Sand from Measured Site Soil Parameters. Offshore Site Investigation and Geotechnics: Integrated Technologies-Present and Future, OnePetro.

Peck, R.B., Hanson, W.E., Thornburn, T.H., 1953. Foundation engineering. Soil Sci. 75 (4), 329.

Randolph, M., Cassidy, M., Gourvenec, S., Erbrich, C., 2005. Challenges of Offshore Geotechnical Engineering. Proceedings of the international conference on soil mechanics and geotechnical engineering, AA Balkema Publishers.

Schertmann, J., 1977. Guidelines for Cone Penetration Test: Performance and Design. Department of Transportation, Federal Highway Administration, Offices of Research and Development (Implementation Division).

Skempton, A.W., 1986. Standard penetration test procedures and the effects in sands of overburden pressure, relative density, particle size, ageing and overconsolidation. Geotechnique 36 (3), 425–447.

Society of Naval Architects Marine Engineers, 1991. Guidelines for Site Specific Assessment of Mobile Jack-up Units. Society of Naval Architects and Marine Engineers.

Society of Naval Architects Marine Engineers, 2008. Guidelines for Site Specific Assessment of Mobile Jack-up Units. Society of Naval Architects and Marine Engineers.

Tang, W.H., 1979. Probabilistic evaluation of penetration resistances. J. Geotech. Eng. Div. 105 (10), 1173–1191.

Teh, K., Cassidy, M., Leung, C., Chow, Y., Randolph, M., Quah, C., 2008. Revealing the bearing capacity mechanisms of a penetrating spudcan through sand overlying clay. Geotechnique 58 (10), 793–804.

Tho, K.K., Leung, C.F., Chow, Y.K., Swaddiwudhipong, S., 2012. Eulerian finite-element technique for analysis of jack-up spudcan penetration. Int. J. GeoMech. 12 (1), 64–73.

Tho, K.K., Leung, C.F., Chow, Y.K., Swaddiwudhipong, S., 2013. Eulerian finite element simulation of spudcan–pile interaction. Can. Geotech. J. 50 (6), 595–608.

Tian, Y., Cassidy, M.J., Randolph, M.F., Wang, D., Gaudin, C., 2014. A simple implementation of RITSS and its application in large deformation analysis. Comput. Geotech. 56, 160–167.

Tolooiyan, A., Gavin, K., 2011. Modelling the cone penetration test in sand using cavity expansion and arbitrary Lagrangian Eulerian finite element methods. Comput. Geotech. 38 (4), 482–490.

Wang, D., Bienen, B., Nazem, M., Tian, Y., Zheng, J., Pucker, T., Randolph, M.F., 2015. Large deformation finite element analyses in geotechnical engineering. Comput. Geotech. 65, 104–114.

Wang, I.T., 2014. Numerical analysis of the dynamic response of slope under the blasting vibration effect. Int. J. Computer Electrical Eng. 6 (4), 351.

White, D., Teh, K., Leung, C., Chow, Y., 2008. A comparison of the bearing capacity of flat and conical circular foundations on sand. Geotechnique 58 (10), 781–792.

Wu, H., Njock, P.G.A., Chen, J., Shen, S., 2019. Numerical simulation of spudcan-soil interaction using an improved smoothed particle hydrodynamics (SPH) method. Mar. Struct. 66, 213–226.

Yi, J.T., Pan, Y.T., Huang, L.Y., Xu, S.J., Liu, Y., Phoon, K.K., 2020. Determination of limiting cavity depths for offshore spudcan foundations in a spatially varying seabed. Mar. Struct. 71, 102723.

Zhu, F., Clark, J.I., Phillips, R., 2001. Scale effect of strip and circular footings resting on dense sand. J. Geotech. Geoenviron. Eng. 127 (7), 613–621.